Electrospun poly(vinylidene fluoride-trifluoroethylene)/zinc oxide nanocomposite tissue engineering scaffolds with enhanced cell adhesion and blood vessel formation

Robin Augustine, Pan Dan, Alejandro Sosnik, Nandakumar Kalarikkal, Nguyen Tran, brice vincent, Sabu Thomas, Patrick Menu, Didier Rouxel

Electrospun poly(vinylidene fluoride-trifluoroethylene)/ zinc oxide nanocomposite tissue engineering scaffolds with enhanced cell adhesion and blood vessel formation

Robin Augustine1,2,§*, Pan Dan3,§, Alejandro Sosnik1, Nandakumar Kalarikkal2,4, Nguyen Tran5, Brice Vincent6, Sabu Thomas2,7, Patrick Menu3, and Didier Rouxel6*

1 Laboratory of Pharmaceutical Nanomaterials Science, Department of Materials Science and Engineering, Technion-Israel Institute of Technology, De-Jur Building, Technion City, Haifa 3200003, Israel
2 International and Inter University Centre for Nanoscience and Nanotechnology, Mahatma Gandhi University, Kottayam, Kerala 686560, India
3 Ingénierie Moléculaire et Physiopathologie Articulaire, UMR 7365 CNRS-Université de Lorraine, Vandoeuvre-lès Nancy F-54500, France
4 School of Pure and Applied Physics, Mahatma Gandhi University, Kottayam, Kerala 686560, India
5 School of Surgery, Faculty of Medicine, Université de Lorraine, Vandoeuvre-lès-Nancy F-54500, France
6 Institut Jean Lamour, UMR 7198 CNRS-Université de Lorraine, Vandoeuvre-lès-Nancy F-54500, France 7 School of Chemical Sciences, Mahatma Gandhi University, Kottayam, Kerala 686560, India
§ These authors contributed equally to this work.
*Address correspondence to Robin Augustine, robin@robinlab.in ; Didier Rouxel, didier.rouxel@univ-lorraine.fr

Abstract

Piezoelectric materials that generate electrical signals in response to mechanical strain can be used in tissue engineering to stimulate cell proliferation. Poly (vinylidene fluoride-trifluoroethylene) (P(VDF-TrFE)), a piezoelectric polymer, is widely used in biomaterial applications. We hypothesized that incorporation of zinc oxide nanoparticles into the P(VDF-TrFE) matrix could promote adhesion, migration, and proliferation of cells, as well as blood vessel formation (angiogenesis). In this study, we fabricated and comprehensively characterized a novel electrospun P(VDF-TrFE)/ZnO nanocomposite tissue engineering scaffold. We analyzed the morphological features of the polymeric matrix by scanning electron microscopy, and utilized Fourier transform infrared spectroscopy, X-ray diffraction, and differential scanning calorimetry to examine changes in the crystalline phases of the copolymer due to addition of the nanoparticles. We detected no or minimal adverse effects of the biomaterials with regard to blood compatibility in vitro, biocompatibility, and cytotoxicity, indicating that P(VDF-TrFE)/ZnO nanocomposite scaffolds are suitable for tissue engineering applications. Interestingly, human mesenchymal stem cells (hMSCs) and human umbilical vein endothelial cells cultured on the nanocomposite scaffolds exhibited higher cell viability, adhesion, and proliferation compared to cells cultured on tissue culture plates or neat P(VDF-TrFE) scaffolds. Nanocomposite scaffolds implanted into rats with or without hMSCs did not elicit

immunological responses, as assessed by macroscopic analysis and histology. Importantly, nanocomposite scaffolds promoted angiogenesis, which was increased in scaffolds pre-seeded with hMSCs. Overall, our results highlight the potential of these novel P(VDF-TrFE)/ZnO nanocomposites for use in tissue engineering, due to their biocompatibility and ability to promote cell adhesion and angiogenesis.

KEYWORDS: scaffolds, electrospinning, poly(vinylidene fluoridetrifluoroethylene), (P(VDFTrFE)), ZnO, angiogenesis, cell adhesion, stem cells

1 Introduction

A wide range of polymeric materials has been suc- cessfully used to create tissue engineering scaffolds, but the search for an ideal scaffold material that can enhance cell adhesion, migration, and proliferation is still underway. An active blood vessel network, which is necessary for the integration of the scaffold with the existing host tissues, has been difficult to achieve with the present technology [1]. Though there are promising strategies to enhance angiogenesis, such as the incorporation of growth factors like vascular endothelial growth factor (VEGF) in scaffolds, their short half-lives limit their usefulness [2]. In addition, such approaches have occasionally resulted in transient efficacy followed by chronic inflammation, fibrosis, and subsequent implant failure [3].

Electrical charges have a beneficial effect on cell adhesion, morphology, and proliferation [4, 5]. Piezo- electric scaffolds, which generate electric signals in response to pressure or vibration, have been used for various tissue engineering applications [6]. Poly (vinylidenefluoride-trifluoroethylene (P(VDF-TrFE)), a copolymer of PVDF, has received special attention among piezoelectric polymers because it easily forms the active piezo β-phase, without additional processing, upon polymerization with small amounts of TrFE [7]. The copolymer has been reported to further undergo crystallization into four different crystalline phases (α, β, γ, and δ) [8]. With the exception of the α-phase, all of the phases are polar. Spontaneous polarization of the γ- and δ-phases leads to the formation of the β-phase, and the α-phase can be converted into the β-phase by mechanical drawing or annealing under high pressure [9].

Electrospun tissue engineering scaffolds based on various biodegradable and non-biodegradable polymers have been extensively studied [10]. The high electric potential and the stretching force applied during electrospinning induce the polarization of P(VDF-TrFE) to form more β-phase crystals than are present in the unprocessed powder [6]. Being a non-biodegradable polymer, P(VDF-TrFE) cannot be recommended for all tissue engineering applications. However, previous studies have demonstrated that P(VDF-TrFE) is a good candidate for neural tissue engineering [11, 12], spinal cord regeneration [13], and skeletal muscle tissue engineering [14]. A recent study demonstrated the feasibility of using electrospun P(VDF-TrFE) scaffolds, in conjunction with stem cell- derived cardiovascular cells, for engineering cardiovas- cular tissues [15].

Zinc oxide (ZnO) nanoparticles have attracted a great deal of attention in recent years because of their multifunctional properties, especially their antibac- terial activity, which could be exploited in specific biomedical interventions to prevent biomaterials- associated infections [16]. ZnO nanostructures, which are also endowed with piezoelectric features [17] as well as the capacity to generate reactive oxygen species (ROS) [18], have found applications in nanomedicine [19]. Our group previously reported that 60-nm ZnO

nanoparticles enhance animal cell proliferation both in vitro and in vivo [20, 21]. Furthermore, another study established that ZnO nanoparticles enhanced the expression of growth factors, like fibroblast growth factor (FGF) and VEGF, which, in turn, promoted cell proliferation and angiogenesis [22]. Although concerns remain regarding the toxicity of ZnO nanoparticles [23, 24], they are being considered for possible clinical application [25]. We designed a tissue engineering scaffold material to elicit robust cell proliferation and angiogenesis by exploiting the piezoelectric properties of both P(VDF- TrFE) and ZnO nanoparticles, as well as the ROS- mediated proliferation induced by ZnO nanoparticles. To the best of our knowledge, the use of electrospun P(VDF-TrFE) fibers containing ZnO nanoparticles in tissue engineering scaffolds has not been reported. In the present work, we generated this novel nano- composite biomaterial and characterized the possible synergistic effects of both components on cell adhesion and angiogenesis.

2 Experimental

2.1 Materials

P(VDF-TrFE) (60:40 molar ratio, Mw ◎ 500,000 g mol-1) was obtained from Piezotech SAS, France. ZnO nanoparticles with average particle size of 60 nm (NanoGard◎) were purchased from Alfa Aesar (UK). Acetone was obtained from Merck (India). Histopaque, polyethyleneimine (PEI), paraformaldehyde and (3-(4,5-dimethylthiazol-2-yl)-2,5-diphenyltetrazolium bromide) (MTT) were purchased from Sigma-Aldrich (USA). Lactate dehydrogenase (LDH) assay kit obtained from Roche (Switzerland). Phalloidin was purchased from Thermo Fisher Scientific (France). Minimum essential medium Eagle-alpha modification (α-MEM) (Lonza) was used for hMSCs culture and endothelial basic medium (Lonza) was used for human umbilical vein endothelial cells (HUVEC) culture. Both media were supplemented with 10% fetal bovine serum (FBS), 100 mg ml-1 Fungizone (Fisher), 100 IU ml-1 penicillin (Sigma-Aldrich) and 200 mM L-glutamine (Sigma-Aldrich) on culture plates. All the reagents used in this study were of analytical grade quality and used without further purification.

2.2 Electrospinning of P(VDF-TrFE)/ZnO nano- composites

Scaffolds of P(VDF-TrFE)/ZnO nanocomposites were fabricated by electrospinning. The electrospinning apparatus was assembled by Holmarc Opto- Mechatronics (India); it consisted of a high-voltage power supply, a syringe pump, and a 10-mL syringe with a 21-gauge needle. A steel rotating (1,000 rpm) mandrel was used as the collector. A 10-cm distance and an applied voltage of 18 kV were maintained bet- ween the needle and the collector. The solution flow rate was precisely maintained at 1.5 mL·h–1 using the syringe pump. P(VDF-TrFE) solutions with different concentrations of ZnO nanoparticles were prepared in acetone. Before they were added to the solution, ZnO nanoparticles were accurately weighed and ultrasonicated for 15 min to achieve complete dispersal. Then, a known quantity of P(VDF-TrFE) in pellet form was added to the above dispersions to achieve a final concentration of P(VDF-TrFE) of 14% w/v, and the mixture was stirred magnetically (12 h) until the pellet complete dissolved. Finally, we electrospun 10 mL of the prepared suspensions with different percentages of ZnO nanoparticles (0%, 0.5%, 1%, 2%, and 4% w/w with respect to the polymer, referred to as P(VDF-TrFE), P(VDF-TrFE)/ZnO-0.5, P(VDF-TrFE)/ZnO-1, P(VDF-TrFE)/ ZnO-2, and P(VDF-TrFE)/ZnO-4, respectively) for 6 h.

After completion of the process, the fibrous scaffolds deposited on the collector were carefully cut and removed using a sharp blade.

2.3 Scanning electron microscopy (SEM) and energy- dispersive X-ray spectroscopy (EDS)

The morphological features of the fabricated scaffolds were visualized with a Philips XL-30 FEG scanning electron microscope at 5 kV (Netherlands). Using a sharp blade, we made 3 mm × 3 mm sections of the scaffolds, which we mounted on SEM sample holders, and subsequently coated with Pt. The average fiber diameter of each sample was measured using ImageJ software. Measurements were made at 100 random positions and the average of these measurements was used to determine the diameter of the fibers. The presence of ZnO nanoparticles in the scaffolds was confirmed by EDS (EDAX, USA) using the Philips XL-30 FEG SEM.

2.4 Fourier transform infrared (FTIR) spectroscopy

FTIR spectra of neat P(VDF-TrFE) and P(VDF-TrFE)/ ZnO nanocomposite scaffolds were obtained with a PerkinElmer spectrum 400 FT-IR spectrometer (USA) with PIKE GladiATR attachment (USA) and DTGS detector on a diamond crystal; spectra were acquired in the 550–1,500 cm−1 range with 15 scans at 4 cm−1 resolution, using Spectrum 400 software 62 (version 6.3).

2.5 X-ray diffraction (XRD)

We used XRD to determine the crystallinity and presence of ZnO nanoparticles in P(VDF-TrFE)/ZnO nanocomposite scaffolds. XRD was recorded in the 2θ range of 20°–25° using a model D8 ADVANCE from Bruker (Germany) with CuKα radiation of 8.04 keV and wavelength of 1.54 Å. The applied voltage was 40 kV and the current was 25 mA.

2.6 Differential scanning calorimetry (DSC)

Calorimetric measurements were performed using a TA Instruments Q200 differential scanning calorimeter (USA). Samples of approximately 5 mg were cut from the neat P(VDF-TrFE) and P(VDF-TrFE)/ZnO nano- composite scaffolds and sealed in 30-μL capacity Al crucible pans. All runs were carried out under a dry nitrogen flow of 20 mL·min–1. Samples were heated from −80 to 200 °C at a rate of 10 °C·min–1. Then, the samples were kept for 1 min at 200 °C to erase the thermal history and cooled to −80 °C. The melting temperature (Tm), the enthalpy of fusion (ΔHf), the ferroelectric-to-paraelectric transition temperature (TF-P), and the enthalpy change during ferroelectric- to-paraelectric transition (ΔHF-P) were calculated from the heating ramp. The crystallization temperature (Tc), the paraelectric-to-ferroelectric transition temperature (TP-F), and the enthalpy change during the paraelectric- to-ferroelectric transition (ΔHP-F) were established from the cooling ramp.

2.7 Porosity measurement

The porosity of the fabricated membranes was measured using the alcohol displacement

method [26]. P(VDF-TrFE) and nanocomposite scaffolds were immersed in 100% ethanol for 48 h until they were saturated, and the percentage of porosity was calculated according to Eq. (1). $P = (W2 - W1)/\varrho V1 \times 100$ (1)

where W1 and W2 are the weight of the scaffolds before and after immersion in ethanol, respectively. V1 is the volume of the scaffold before immersion in ethanol, and ϱ is the density of ethanol. The experiment was repeated on three sets of samples and the porosity was expressed as mean ± standard deviation (S.D.) (n = 3).

2.8 Blood compatibility studies

Since the tissue engineering scaffolds are expected to come into direct contact with blood, assessment of their hemocompatibility is essential. We performed blood cell aggregation and hemolysis tests, according to published protocols, with minor modifications [27]. After we obtained informed consent, we collected human blood samples (approximately 10 mL) from healthy volunteers into tubes containing 3.8% sodium citrate at a 9:1 ratio (blood:anticoagulant). Normal saline and PEI were used as the negative and positive controls for hemolysis, respectively. Both neat P(VDF-TrFE) and P(VDF-TrFE)/ZnO nanocomposite scaffolds were cut into 1 cm × 1 cm pieces and sterilized by dipping in 70% alcohol for 20 min followed by UV irradiation for 20 min. The samples were incubated overnight in 1 mL of sterile phosphate buffered saline (PBS) solution and the resulting solutions were used for red blood cell (RBC) and white blood cell (WBC) aggregation, platelet activation, and hemolysis tests.

2.8.1 Blood cell aggregation study

For the RBC aggregation studies, blood was centri- fuged at 700 rpm for 10 min to separate the RBCs from the blood plasma. The cell fraction was washed twice with saline and diluted with PBS (1:4). Then, 2 mL of the diluted RBCs was added to the PBS solution generated by overnight incubation with the scaffolds, and kept at 37 °C for 20 min. The diluted RBCs were also incubated with the negative and positive control solutions. To assess WBC compatibility, cells were isolated from anticoagulated blood overlaid on Histopaque® by centrifugation (15 min at 800 rpm). The collected WBCs were incubated with the PBS solution generated by overnight incubation with the scaffolds for 20 min at 37 °C. WBCs were also incubated with the positive and negative controls. After incubation, both RBCs and WBCs were isolated by centrifugation, resuspended in PBS, and mounted on wet slides. Images were captured by optical microscope (Leica DMIRB, Germany).

2.8.2 Platelet aggregation

Platelets were isolated from anticoagulated blood (1 mL) overlaid on Histopaque® (1 mL) in order to separate RBCs and WBCs into distinct layers, then centrifuged for 15 min at 800 rpm at room temperature; platelets were separated into the topmost layer above the WBC fraction. The collected platelets were incubated with the PBS solutions generated by overnight incubation with the scaffolds for 20 min at 37 °C. The platelets were also incubated with the positive and negative controls. Images were captured by optical microscope (Leica DMIRB, Germany).

2.8.3 Hemolysis assay

Hemolysis assays were carried out with the P(VDF-TrFE) and P(VDF-TrFE)/ZnO scaffolds. In brief, 100 μL of the separated blood was diluted with 800 μL of saline. To this diluted blood, we added 100 μL of each PBS solution generated by overnight incubation with the scaffolds. We used normal saline as the negative control (no hemolysis) and distilled water as the positive control (complete hemolysis). The samples were incubated for 30 min at 37 °C and centrifuged at 700 rpm for 5 min. The absorbance (optical density, OD) was measured at 541 nm using a UV–Vis spectrophotometer (Shimadzu double-beam spectrophotometer, Model 1700, Japan). The percentage of hemolysis (% Hemolysis) was calculated using Eq. (2).

% Hemolysis = (OD of sample − OD of negative control)/ (OD of positive control – OD of negative control) (2)

2.9 Cell compatibility and cell attachment

We used hMSCs and HUVECs to assess cell bio- compatibility with and attachment to the scaffolds. Fresh human umbilical cords were obtained with informed consent after full-term births (cesarean section or vaginal delivery) using the guidelines approved by the University Hospital Center of Nancy (France). HUVECs and hMSCs were isolated and expanded as previously reported [28]. HUVECs (passage 2) and hMSCs (passage 4) were seeded on neat P(VDF-TrFE) and P(VDF-TrFE)/ZnO nano- composite scaffolds at 50,000 cells·cm–2 and cultured with appropriate media for 24 h. To visualize cell attachment, samples were fixed with 4% parafor- maldehyde for 15 min, permeabilized with 0.5% w/v Triton X-100 solution for 15 min, then cell cytoskeletons were stained with phalloidin and nuclei were stained with DAPI. Images were taken with a fluorescent microscope (Leica DMI3000 B, Germany). To assess the compatibility of hMSCs and HUVECs with the scaffolds, MTT and LDH assays were carried out according to the corresponding protocols provided by the manufacturers (n = 3).

2.10 In vivo implantation studies

Implantation studies to determine the biocompatibility and biological performance of the nanocomposite scaffolds in vivo were carried out in Wistar rats. All animal experiments were carried out after authorization from the regional animal ethics committee in France (APAFIS #1123-2015070711576639V3). Based on the in vitro cell culture studies, P(VDF-TrFE), P(VDF-TrFE)/ ZnO-1, and P(VDF-TrFE)/ZnO-2 were selected for animal studies. Before implantation, all scaffolds were cut into 1 cm × 1 cm pieces, then sterilized with 70% alcohol for 20 min followed by UV radiation for 20 min. One set of scaffolds was seeded with hMSCs (50,000 cells·cm–2) and allowed to grow for 24 h prior to animal implantation. In order to track these cells, hMSCs were labeled with 1,1′-dioctadecyl-3,3,3′,3′-tetramethylindocarbo-cyanine perchlorate (DiI, D282, Invitrogen, France). A total of 6 rats (male, 231 ± 13 g) were used. Anesthesia was induced by inhalation of 4% isoflurane (Isovet, France) and maintained in 1.5% isoflurane. Scaffolds were implanted subcutaneously in the abdominal region. After 7 and 21 days of im- plantation, the implantation site was reopened and the scaffolds were visually inspected for immune reactions and angiogenesis. Scaffolds were then explanted for cell tracking and histological evaluation. Samples were cut into transverse and cross-sections, and stained with hematoxylin-eosin-saffron and Masson's trichrome. Stained sections were used to assess in vivo bio- compatibility and the formation

of blood vessels. The stained sections were examined with a Leica DMI3000 B inverted light microscope.

2.11 Statistical analysis

Data are presented as mean ± S.D. For fiber diameter, MTT, and LDH evaluation, statistical significance was determined by analysis of variance (ANOVA) followed by Student's t-test between each group; p-values less than 0.05 were defined as statistically significant.

3 Results

3.1 Morphology of scaffolds

In this study, we aimed to develop a P(VDF-TrFE)/ ZnO nanocomposite scaffold by means of an electrospinning technique. A schematic representation of the fabrication process is shown in Scheme 1.

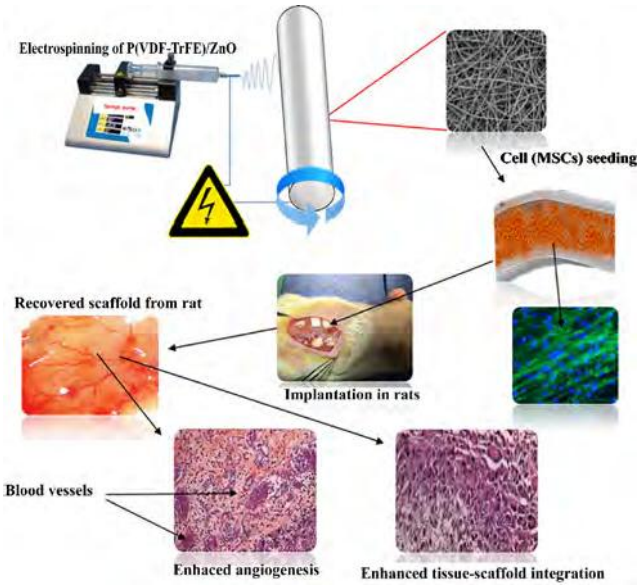

Scheme 1 Schematic representation of the production of electrospun P(VDF-TrFE)/ZnO nanocomposite scaffolds, hMSC seeding of scaffolds, and implantation in rats (figures are not to scale).

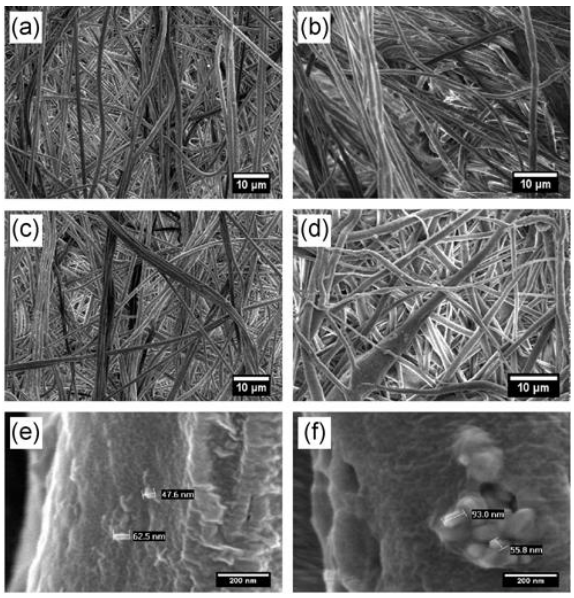

Figure 1 SEM micrographs showing the morphology of electrospun (a) P(VDF-TrFE), (b) P(VDF-TrFE)/ZnO-1, (c) P(VDF- TrFE)/ZnO-2, and (d) P(VDF-TrFE)/ZnO-4. The images in (e) and (f) are higher magnification images of (b) and (d), respectively.

Representative morphological features of neat P(VDF-TrFE) and P(VDF-TrFE)/ZnO nanocomposite scaffolds are presented in Fig. 1. As expected, scaffolds were highly porous with randomly oriented fibers and good pore interconnectivity. In addition, both P(VDF-TrFE) and P(VDF-TrFE)/ZnO nanocomposite scaffolds appeared to have almost uniform fiber diameter. Higher magnification micrographs confirmed the presence of well-dispersed ZnO nanoparticles. In the scaffolds with a low ZnO nanoparticle load, the

particles were mainly embedded and homogeneously dispersed in the P(VDF-TrFE) fibers (Fig. 1(e)). However, an increase in the ZnO content resulted in the for- mation of nanoparticle agglomerates that protruded from the fibers and were visible on the surface (Fig. 1(f)).

To further understand the impact of the incorporation of ZnO nanoparticles on the fibers, we measured the diameter of the fibers (Table 1). In neat P(VDF-TrFE) scaffolds, fibers had an average diameter of 1,035 nm. The fiber diameter of P(VDF-TrFE)/ZnO nano- composites varied as the nanoparticle concentration increased. In P(VDF-TrFE)/ZnO-1 scaffolds, the change was marginal and did not reach statistical difference ($p = 0.68$). However, for P(VDF-TrFE)/ZnO-2, the diameter was significantly larger than the neat counterpart ($p = 0.0004$). Further increases in the ZnO nanoparticle content up to 4% w/w in the P(VDF-TrFE) scaffolds led to additional increases in the fiber diameter ($p < 0.0001$ in both cases).

Table 1. Effect of ZnO concentration on the fiber diameter of P(VDF-TrFE) scaffolds.

Sample	**Fiber average diameter ± S.D. (nm)**
P(VDF-TrFE)	1035 ± 331
P(VDF-TrFE)/ZnO-1	1052 ± 275

P(VDF-TrFE)/ZnO-2	1185 ± 249
P(VDF-TrFE)/ZnO-4	1227 ± 301

3.2 EDS

EDS spectra of electrospun P(VDF-TrFE) scaffolds and their nanocomposite counterparts were used to confirm the presence of ZnO nanoparticles in the polymer matrix (Fig. 2). Neat P(VDF-TrFE) scaffolds displayed sharp low-energy peaks that could be assigned to the elements carbon (Kα radiation with 0.277 keV) and fluorine (Kα radiation with 0.677 keV) (Fig. 2(a)). Similar results have been reported elsewhere [29]. In the case of the nanocomposites, the characteristic signals of Zn were observed at energy levels 1.01 keV (Lα), 8.63 keV (Kα), and 9.5 keV (Kβ) (Figs. 2(b)–2(d)).

These peaks were in full agreement with our previous results [20]. Importantly, there was a marked increase in the intensity of the three characteristic peaks of Zn in the scaffolds with increased ZnO nanoparticle content. Oxygen and fluorine showed characteristic Kα emissions at 0.525 and 0.677 keV, respectively. Thus, it was not possible to discern the peaks corresponding to the oxygen from the ZnO nanoparticles due to the overlapping high-intensity fluorine peaks belonging to P(VDF-TrFE).

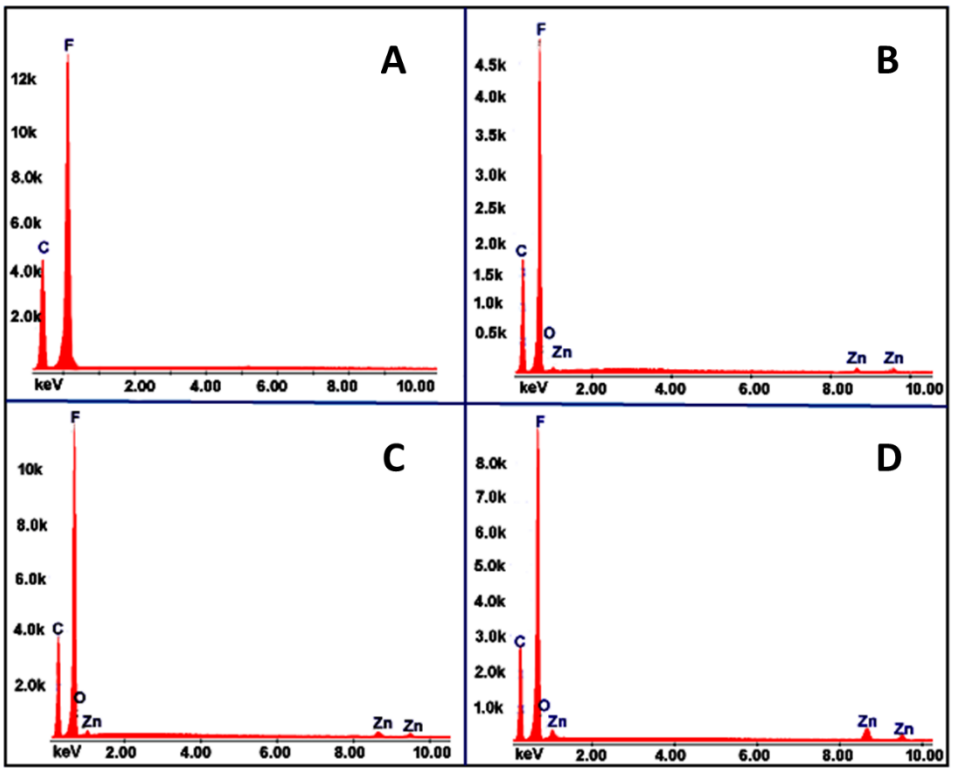

Fig. 2. Representative EDS spectra of (A) electrospun P(VDF-TrFE), (B) P(VDF-TrFE)/ZnO-1, (C) P(VDF-TrFE)/ZnO-2, and (D) P(VDF-TrFE)/ZnO-4.

3.3 Crystalline phase analysis

3.3.1 FTIR

The FTIR spectra of the electrospun neat scaffolds are shown in Fig. 3(a). The 1,283 cm–1 band was assigned to the symmetric CF2 stretching vibration coupled to the backbone stretching and bending vibrations corresponding to trans isomer sequences that are four or more units long in the extended chain or β-phase structure [30, 31]. The two bands near 845 cm–1 and the band at 1,283 cm–1 belonged to long sequences of at least three trans isomers [30]. They were assigned to a mixed mode of CH2 rocking [32] and CF2 asymmetric stretching vibration parallel to the chain axis [33]. Characteristic peaks at 1,400, 1,284, and 845 cm–1 corresponded to the electroactive β-phase, whereas a very weak and broad band at 975 cm–1 and an ill-defined peak around 613 cm–1 in neat P(VDF–TrFE) scaffolds were due to the non-polar α-phase [34, 35]. It is worth noting that the characteristic ⌾-phase bands at 1,455, 1,430, 1,385, 1,212, 1,152, 976, 855, and 796 cm–1 were completely absent. The same was true of the γ-phase peak at 1,232 cm–1. Incorporation of ZnO nanoparticles did not result in a considerable shift of any of the characteristic IR bands. Since we conducted the analysis by attenuated total reflectance, we were able to obtain semi-quantitative information regarding the relative amounts of the different crystalline phases (Fig. 3(b)). We focused on the spectrum region between 1,500 and 1,300 cm–1, and analyzed the variation in the intensity of the band at 1,400 cm–1, which represents the β-phase [35]. The intensity of the β-phase band at 1,400 cm–1 increased due to the incorporation of ZnO nanoparticles, and P(VDF-TrFE)/ ZnO-2 had the most substantial increase. Overall, these findings stress the fundamental role of the production procedure in the microstructural properties of the polymer in the final product and the ability to fine-tune them by incorporating solid nanoparticles that serve as nucleation and crystallization sites during the formation of the fibers.

3.3.2 XRD

Crystallinity in polymeric biomaterials determines their physical, mechanical, and biological properties. P(VDF-TrFE) is a semi-crystalline copolymer that consists of an amorphous matrix with an embedded ferroelectric crystalline β-phase, composed of a quasi- hexagonal, close-packed orthorhombic mm2 structure [36]. The XRD patterns of electrospun P(VDF-TrFE)/ZnO nanocomposite scaffolds revealed that the main diffraction peak of the P(VDF-TrFE) and P(VDF-TrFE)/ ZnO nanocomposite scaffolds was at 2⌾ = 19.9° (110) (Fig. 3(c)). This diffraction peak could be assigned to the (200) and (110) planes of the ⌾-phase [37]. No other specific diffraction peaks corresponding to the ⌾-, ⌾-, or γ-phases were identified. Instead, a broad peak covering the 2⌾ region between 16° and 22°, with a maximum at 19.9°, was observed. When ZnO nanoparticles were incorporated, the corresponding diffraction peaks of the ZnO nanoparticles were apparent at 2⌾ values of 31.7°, 34.3°, 36.3°, 47.3°, 56.6°, and 63.8° (Fig. 3(c)). Moreover, the intensity of the signals increased correspondingly with ZnO content.

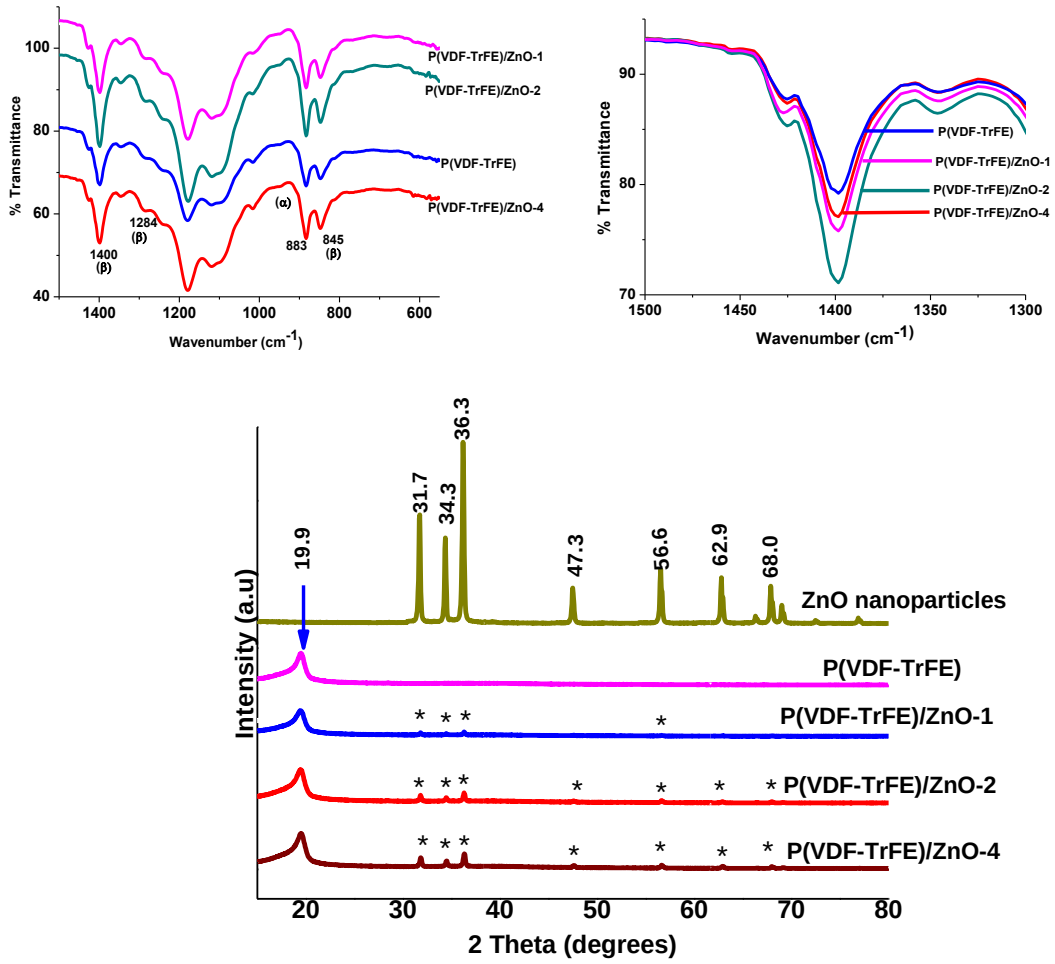

Fig. 3. (A, B) FTIR spectra of (A) neat P(VDF-TrFE) and P(VDF-TrFE)/ZnO nanocomposite scaffolds with growing concentration of ZnO nanoparticles and (B) an enlarged view of the band at 1400 cm-1 which indicates the variation of relative intensity of ◎-phase in the nanocomposites. (C) XRD patterns of the scaffolds where (*) represents the diffraction patterns of ZnO nanoparticles in nanocomposite scaffolds.

3.3.3 DSC

To gain deeper insight into the thermal and crystal properties of the electrospun P(VDF-TrFE) scaffolds with and without ZnO nanoparticles, we analyzed the samples by DSC. We observed two endothermic peaks for all fabricated scaffolds. The first peak around 67 °C corresponded to the TF-P of the copolymer, and the second transition near 158 °C was the Tm of the polymer [38]. This broad endothermic peak during melting could be described as a superposition of the melting peaks for the lower-melting ◎-phase and the higher melting ◎-phase (Fig. S2 in the ESM). We did not detect considerable variation in the Tm and TF-P upon incorporation of ZnO nanoparticles into the fibers (Table 2). Similar to their properties during the heating process, during the cooling process, neat P(VDF-TrFE) and ZnO-loaded scaffolds exhibited exothermic peaks of Tc and TP-F at approximately 141–143 and 59–61 °C, respectively. In P(VDF-TrFE)/ZnO scaffolds, we did not observe variation in Tc or TP-F. Interestingly, ΔHc slightly decreased in scaffolds with low ZnO nano- particle content. Similarly, ΔHP-F considerably increased with growing concentrations of ZnO nanoparticles,

up to 2% w/w ZnO. However, a further increase in ZnO content resulted in a decrease in ΔHP-F.

Table 2. Effect ZnO nanoparticles on the thermal behavior of P(VDF-TrFE) scaffolds.

Samples	T_m (°C)	ΔH_f (J/g)	T_{F-P} (°C)	ΔH_{F-P} (J/g)	T_c (°C)	ΔH_c (J/g)	T_{P-F} (°C)	ΔH_{P-F} (J/g)
Neat P(VDF-TrFE)	158	25	67	10	143	27	61	9
P(VDF-TrFE)/ZnO-1	158	23	68	13	142	24	60	11
P(VDF-TrFE)/ZnO-2	159	23	68	12	141	24	59	12
P(VDF-TrFE)/ZnO-4	159	23	67	9	142	26	60	9

3.4 Porosity measurements

The porosity of the fabricated P(VDF-TrFE)/ZnO nanocomposite scaffolds was evaluated using the alcohol displacement method (Table 3). The fabricated membranes all had 88%–92% porosity. Nanofiller addition had no significant effect on the porosity of the scaffolds.

Table 3. Porosity of P(VDF-TrFE) membranes in percentage.

Sample	Porosity (%)
P(VDF-TrFE)	92.2 ± 1.5
P(VDF-TrFE)/ZnO-0.5	90.4 ± 1.8
P(VDF-TrFE)/ZnO-1	88.7 ± 2.2
P(VDF-TrFE)/ZnO-2	91.3 ± 2.1
P(VDF-TrFE)/ZnO-4	90.6 ± 1.2

3.5 Blood cell aggregation, platelet activation, and hemolysis studies

Tissue engineering scaffolds are in direct contact with blood at the implantation site. Thus, scaffold- induced aggregation of blood cells would preclude the use of a particular biomaterial. We studied the aggregation behavior of RBCs, WBCs, and platelets upon incubation with aqueous extracts of the pristine and modified scaffolds (Fig. 4). We did not observe aggregation of blood cells that were incubated with the aqueous scaffold extracts or with saline solution (negative control). In contrast, incubation with PEI (positive control) induced aggregation. Platelet acti- vation is the initial step in blood coagulation. Neat P(VDF-TrFE) scaffold and nanocomposite scaffold extracts did not activate platelets. The positive control, however, caused platelet aggregation and formation of circular clumps (Fig. 4).

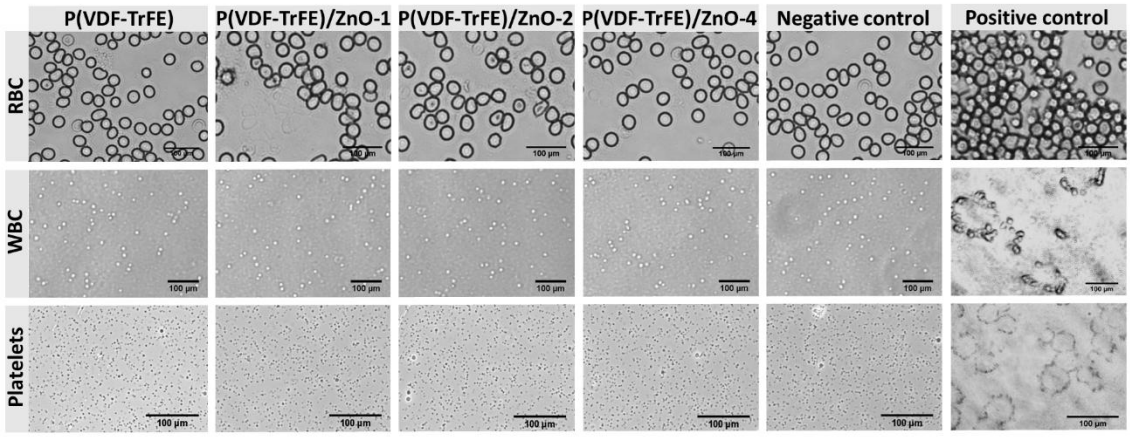

Fig. 4. RBC, WBC and platelet aggregation upon contact with P(VDF-TrFE), P(VDF-TrFE)/ZnO-1, P(VDF-TrFE)/ZnO-2 and P(VDF-TrFE)/ZnO-4 extracts. PBS and PEI were included as negative and positive control.

Hemolysis is another critical property to be tested in the determination of the blood compatibility of biomaterials. We calculated the hemocompatibilty of the scaffolds with respect to a negative control (normal saline, assumed to be 0% hemolytic) and a positive control (double distilled water, assumed to be 100% hemolytic). The hemolysis test results for the P(VDF-TrFE) and P(VDF-TrFE)/ZnO nanocomposite scaffolds are shown in Table 4. All tested samples had comparable hemolysis ($p > 0.05$).

Table 4. Percentage of hemolysis due to P(VDF-TrFE) and P(VDF-TrFE)/ZnO nanocomposite scaffolds.

Sample	**%Hemolysis** ± S.D.
Neat P(VDF-TrFE)	0.3 ± 0.04
P(VDF-TrFE)/ZnO-0.5	0.2 ± 0.01
P(VDF-TrFE)/ZnO-1	0.3 ± 0.02
P(VDF-TrFE)/ZnO-2	0.3 ± 0.04
P(VDF-TrFE)/ZnO-4	0.3 ± 0.07
Negative control	0
Positive control	100

3.6 In vitro performance of the scaffolds

To further confirm the applicability of the developed scaffolds for tissue engineering, we assessed cell viability, cytotoxicity, and attachment with HUVECs and hMSCs. The viability of HUVECs grown in the presence of P(VDF-TrFE) was comparable to the viability of those grown on commercial cell culture plates (Fig. 5(a)). Interestingly, HUVECS grown on P(VDF-TrFE)/ZnO-1 and P(VDF-TrFE)/ZnO-2 scaffolds had significantly higher viability than the controls. In contrast, P(VDF-TrFE)/ZnO-4 was slightly cytotoxic. We found a similar trend with hMSCs (Fig. 5(b)). Thus, the viability of cells grown in cell culture plates, P(VDF-TrFE) scaffolds, and P(VDF-TrFE)/ZnO-1 scaffolds were comparable. Similar to the HUVECs, hMSCs grown on P(VDF-TrFE)/ZnO-2 were more viable than controls, or cells grown on P(VDF-TrFE)/ZnO-1 and P(VDF-TrFE)/ZnO-4 scaffolds. Finally, the viability of

hMSCs in the presence of P(VDF-TrFE)/ZnO-4 was substantially lower than the viability of those grown in the control conditions.

We used the LDH assay as a complementary study to reveal cell membrane damage that could result in cell death at a later stage. Neat P(VDF-TrFE), P(VDF-TrFE)/ZnO-1, and P(VDF-TrFE)/ZnO-2 scaffolds were largely non-toxic to both HUVECs and hMSCs (Figs. 5(c) and 5(d)). In contrast, P(VDF-TrFE)/ZnO-4 scaffolds were cytotoxic to HUVECs, but not hMSCs.

To evaluate the ability of the scaffolds to allow end- othelial cell adhesion, a prerequisite for angiogenesis, HUVECs or hMSCs were seeded on P(VDF-TrFE) and nanocomposite scaffolds, then allowed to grow for 24 h. Previous reports have indicated that hMSCs can differentiate into endothelial cells [39]. Figure 5(e) shows the adhesion of both cell types to P(VDF-TrFE) and P(VDF-TrFE)/ZnO nanocomposite scaffolds (additional micrographs of crystal violet-stained cell- seeded scaffolds are included in Fig. S3 in the ESM).

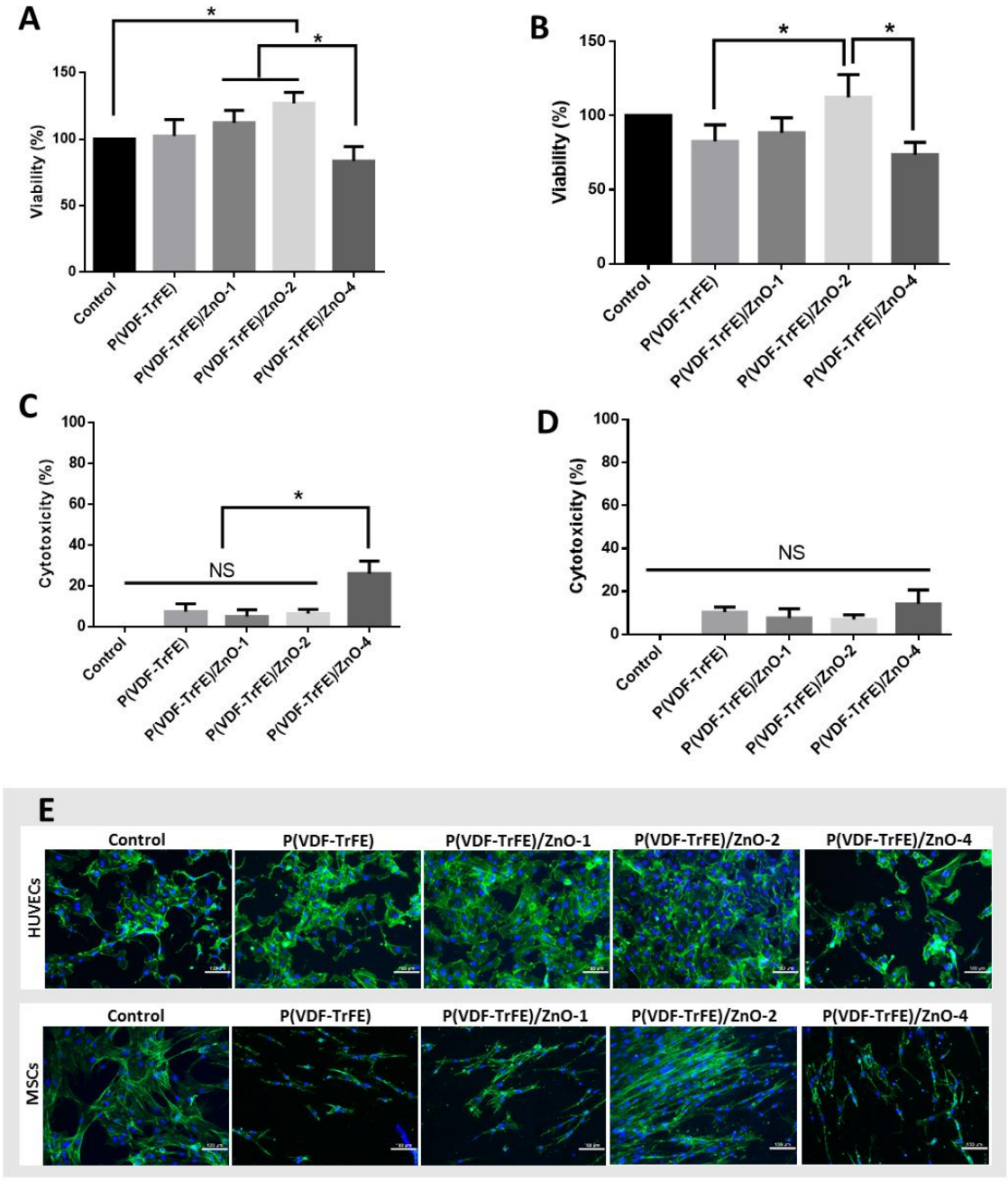

Fig. 5. In vitro cell compatibility and cytotoxicity studies. (A, B) Cell viability of (A) HUVECs and (B) hMSCs on the scaffolds, as determined by MTT assay. (C, D) Cytotoxicity of (C) HUVECs and (D) hMSCs, as determined by LDH assay. Data are mean ± SD (n=3, * $p < 0.05$ indicate statistically significant differences using ANOVA and followed by a Tukey test between all groups). NS, no significance. Cell attachment of HUVECs and hMSCs (E) on the scaffolds after 24 hours of culture (50000 cells/cm2 seeded).

We observed similar proliferation and spread morphology of HUVECs on neat P(VDF-TrFE) scaffolds and control plates. Unlike on P(VDF-TrFE)/ZnO-4 scaffolds, cell adhesion and proliferation were considerably higher on P(VDF-TrFE)/ZnO-1 and P(VDF-TrFE)/ZnO-2 scaffolds. Compared with cells grown under control conditions, hMSCs grown on neat P(VDF-TrFE) scaffolds and P(VDF-TrFE)/ZnO-1 scaffolds demonstrated slightly less cell adhesion and spreading. However, P(VDF-TrFE)/ZnO-2 scaffolds supported confluent

growth of hMSCs with elongated morphology. As observed before, the decrease in cell proliferation was most notable for cells grown on P(VDF-TrFE)/ZnO-4 scaffolds compared to those grown on the neat P(VDF-TrFE) and nanocomposite scaffolds with lower ZnO nanoparticle content.

3.7 In vivo angiogenesis in scaffolds

Based on the results of the in vitro cell culture studies, we selected the P(VDF-TrFE), P(VDF-TrFE)/ZnO-1, and P(VDF-TrFE)/ZnO-2 scaffolds for subcutaneous implantation studies to evaluate their in vivo per- formance (Fig. S4(a) in the ESM). We did not observe visual inflammation or severe immunological responses at the implantation sites of any of the scaffolds after 7 and 21 days (Fig. S4(b) in the ESM).

Macroscopic observation indicated the formation of more blood vessels on the scaffolds containing ZnO nanoparticles than on neat P(VDF-TrFE) scaffolds. We observed highly branched vasculature in the P(VDF-TrFE)/ZnO-2 scaffolds that were pre-seeded with hMSCs (Figs. 6(a) and 6(b)). Tracking of fluores- cently labeled hMSCs confirmed their presence in the scaffolds even after 21 days of implantation (Fig. 6(c)). Histological evaluation of scaffold cross-sections 7 days after implantation revealed extensive networks of collagen fibers throughout the scaffolds (Fig. 7(a)). Although we observed some inflammatory cells, we did not detect intergroup differences. At 7 days post- implantation, we observed neovascularization in the tissue adjacent to the scaffolds; the number of newly formed blood vessels depended on percentage of ZnO nanoparticles in the scaffolds and the presence of hMSCs (Fig. 7(c)). At 21 days post-implantation, we observed the in-growth of blood vessels, especially on nanocomposite scaffolds pre-seeded with hMSCs (Fig. 7(b)). Notably, throughout the period of study, the best angiogenic responses were observed with P(VDF-TrFE)/ZnO-2 scaffolds that had been pre- seeded with hMSCs (Figs. 7(c) and 7(d)). Transverse and cross-sections of the scaffolds confirmed that angiogenesis took place throughout the sample, not only on the surface (Figs. S5 and S6 in the ESM).

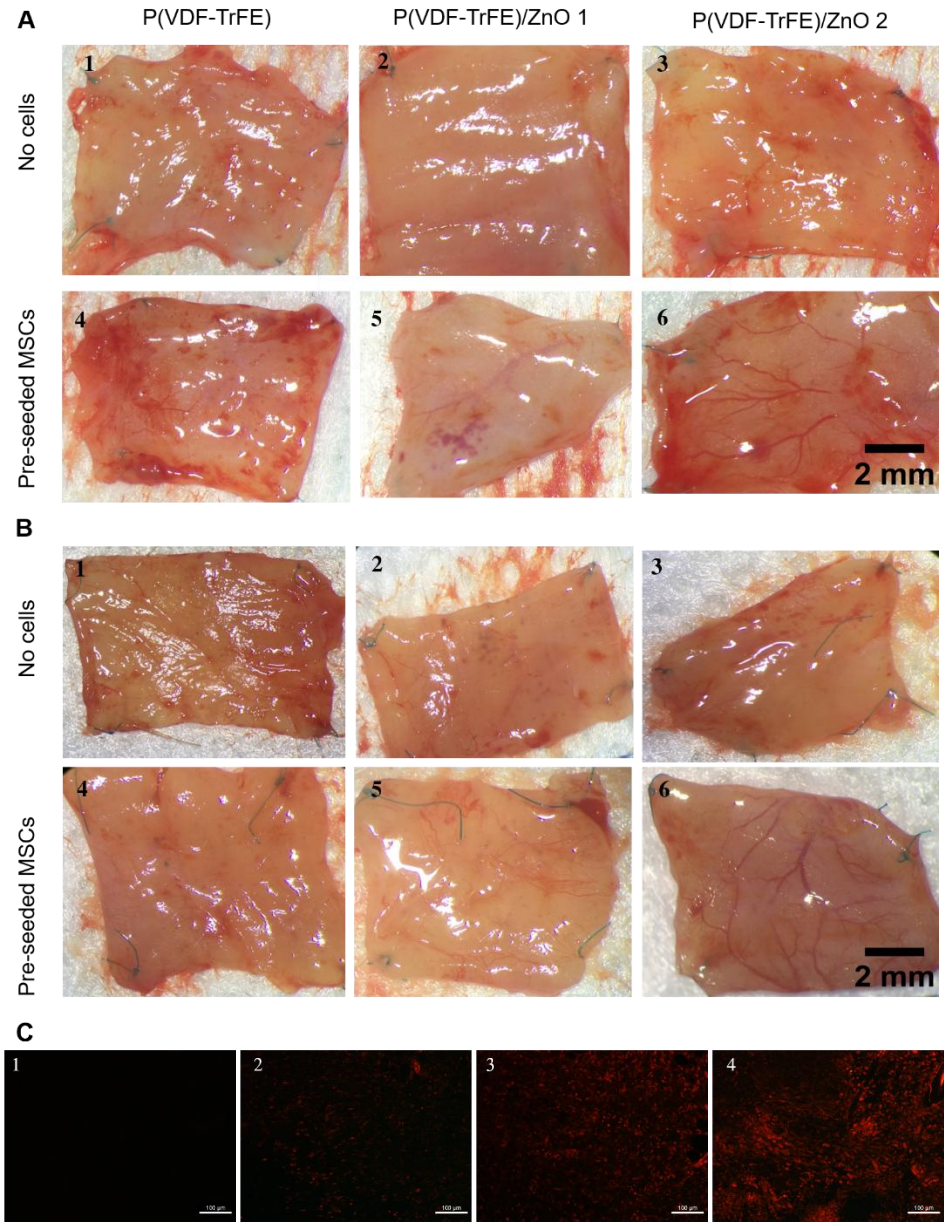

Fig. 6. Observation on scaffolds after subcutaneous implantation. Macroscopic inspection of explanted samples at 7th day (A) and 21st day (B) after implantation. (C) Fluorescent cell tracking at 21st day after implantation. hMSCs were confirmed by pre-labeled DiI after eliminating the influence of autofluorescence of scaffolds and tissue. (C1) Scaffold without cells as control, (C2) P(VDF-TrFE), (C3) P(VDF-TrFE)/ZnO-1, (C4) P(VDF-TrFE)/ZnO-2.

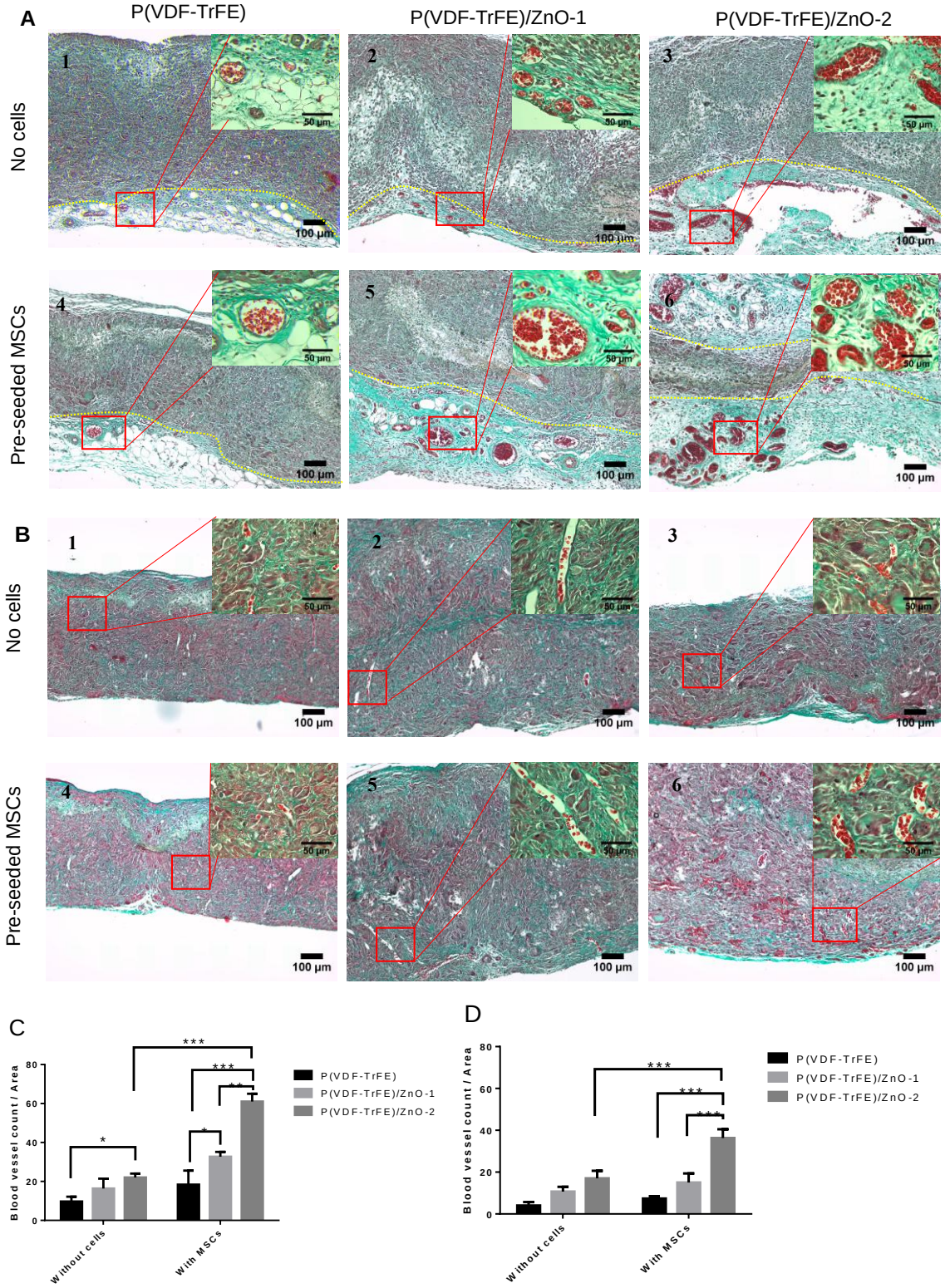

Fig. 7. Histological analysis of scaffolds after implantation. Scaffolds were cross cut and stained with Masson trichrome. (A) 7th day after implantation, blood vessels were observed in connective tissue adjacent to scaffolds (distinguished by yellow dash lines).

Collagen was found in all scaffolds (green). (B) Extensive angiogenesis was observed throughout the scaffolds after 21st day of implantation. Quantitative analysis of number of blood vessels in tissue adjacent to scaffolds after 7 days (C) and 21 days (D) of implantation.

(n=3, 6 areas (1.3×1mm/area) of each cross section sample were randomly selected, blood vessels with diameter larger than 8μm were counted, ***p< 0.001)

4 Discussion

Synthetic biomaterials are being developed at a rapid pace for therapeutic applications and basic biological studies [40]. Their popularity is mostly due to ease of manipulation, as well as the ability to tailor their properties for specific tissue engineering applications and mimic the natural extracellular matrix environ- ment to support cell growth (e.g. stem cells); synthetic biomaterials can also be produced on an industrial scale in a reproducible manner [41]. Recently, synthetic biomaterials have begun to incorporate molecular cues that control their interactions with the biological environment.

P(VDF-TrFE) has been recognized for its potential in tissue engineering for over a decade [42]. P(VDF- TrFE) and its nanocomposite copolymers are widely appreciated because of their piezoelectric properties and potential in tissue engineering [43, 44]. Here, we reported the synthesis of P(VDF-TrFE) scaffolds con- taining ZnO nanoparticles by electrospinning.

Detailed morphological and spectroscopic characteri- zations confirmed the presence of ZnO nanoparticles in P(VDF-TrFE) fibers. The highly porous morphology and randomly oriented fibers of the scaffolds are highly promising for cell adhesion. We observed a slight increase in fiber diameter due to the incor- poration of increasing concentrations of nanoparticles. These results are in agreement with our previous studies [20]. The increase in fiber diameter may be due to the increased viscosity of the spinning solution caused by the presence of nanofiller agglomerates [45, 46]. Lee and coworkers reported that electrospun P(VDF-TrFE) scaffolds with micron-sized fibers are more effective for tissue engineering applications due to higher cell growth [12]. All of the scaffolds in this study possessed micrometer-sized fibers.

Once an engineered scaffold is implanted in vivo, a series of complex events will be initiated, including cell adhesion, migration, proliferation, and scaffold- native tissue integration at the implantation site. The electric potential in the injured tissue has been pro- posed to play a fundamental role in tissue repair [47]. Piezoelectric scaffolds can convert ambient mechanical energy into electric signals, which enhance cell responses [48]. FTIR analysis indicated that the relative abundance of electroactive β-phase material in nanocomposite scaffolds was higher than in neat P(VDF-TrFE) scaffolds. XRD analysis further confirmed the presence of ZnO nanoparticles in the nano- composite scaffolds, as indicated by more intense ZnO signals. These results confirmed that ZnO nanoparticles were successfully incorporated into the polymer matrix during the electrospinning process without adversely affecting the formation of the piezoelectric β-phase.

DSC analysis demonstrated that the incorporation of ZnO nanoparticles into the fibers did not affect the Tm and TF-P owing to retention of the ferroelectric crystalline fraction or the lamellar thickness of the crystalline domains in the nanocomposite copolymers [37]. The analysis demonstrated that the lower percentages of ZnO nanoparticles in P(VDF-TrFE) did not substantially alter the amount of crystalline phase in the polymer matrix. During the cooling process, neat P(VDF-TrFE) scaffolds exhibited a Tc and TP-F that are comparable with those reported in the literature [49]. The slight decrease in both Tc and TP-F observed for the nanocomposites implies that they crystallized at lower temperatures than the neat P(VDF-TrFE). The ΔHF-P endothermic peak was weighted toward higher temperatures, which is an indication of a higher ratio of ◎-phase to ◎-phase in these samples [50]. This characteristic might further improve the performance of the scaffolds in vivo. For example,

Guo et al. reported that electrospun polyurethane/PVDF piezoelectric composites promote cell adhesion better than the pure polyurethane counterpart [51]. Our FTIR and DSC results previously indicated that the incorporation of ZnO nanoparticles increased the crystalline β-phase in the electrospun biomaterials [52]. These findings suggested that the enhanced electroactive phase in the P(VDF-TrFE)/ ZnO scaffolds could be one of the reasons for improved cell adhesion [53]. All of the nanocomposite scaffolds, irrespective of ZnO nanoparticle concentration, have shown adequate porosity to facilitate cell migration, nutrient supply, and blood vessel penetration [54].

Since P(VDF-TrFE) scaffolds could eventually be used in tissue engineering applications involving direct contact with blood, we confirmed their com- patibility with RBCs and WBCs. In addition, we found that platelets did not undergo aggregation after contact with extracts from samples containing up to 4% w/w ZnO nanoparticles. Moreover, all the aqueous scaffold extracts induced <1% hemolysis, the upper limit for medical devices that will come into contact with blood as defined by ASTM (ASTM Standard, F756-08). The results of the blood cell aggregation and hemolysis tests indicate that P(VDF- TrFE)/ZnO nanocomposite scaffolds containing up to 4% w/w ZnO nanoparticles are compatible with blood cells and suitable for the fabrication of various tissue engineering scaffolds.

We studied the interaction of the scaffolds with cells in vitro to select the best prototypes for in vivo characterization. In this study, we demonstrated that the incorporation of 1%–2% w/w of ZnO nano- particles increased the attachment of both HUVECs and hMSCs to P(VDF-TrFE) scaffolds. Apart from the piezoelectric effect of P(VDF-TrFE), ZnO nanoparticles are known to play a major role in cell adhesion and proliferation [55, 56]. However, P(VDF-TrFE)/ZnO-4 scaffolds were slightly cytotoxic, probably due to cell membrane damage mediated by the nanofiller agglomerates that were more exposed at the nanofiber surface in the scaffolds with higher ZnO content [22, 57]. It is important to bear in mind that differences in the cytotoxic concentrations of ZnO nanoparticles that have been reported in the literature might be due to variation in the properties of the nanoparticles (e.g. size, size distribution, shape, and purity) and the polymer matrix used. Previous studies have shown that the size and shape of ZnO nanoparticles could influence their cytotoxic effects [58, 59]. Although a detailed study on the effects of the size and morphology of ZnO nanoparticles on cell interactions with P(VDF-TrFE) fibers is beyond suggesting that they could be utilized for the development of various tissue engineered products.

Vascularization of a tissue engineering scaffold is one of the most important events that determines its ultimate success (or, conversely, failure). Our results demonstrated a higher degree of blood vessel sprouting in nanocomposite scaffolds. At an early stage after implantation, blood vessels were found in adjacent tissue; at 21 days post-implantation, blood vessels began to penetrate the scaffold. Unlike the neat scaffolds, where very few blood vessels formed even after 21 days of implantation, significantly more capillaries were observed in P(VDF-TrFE)/ZnO nano- composites ($p < 0.001$). ZnO nanoparticles can play a crucial role in the promotion of angiogenesis [61]. Scaffolds seeded with hMSCs have also been reported to enhance angiogenesis, as the cells secrete soluble angiogenic signaling molecules [62]. We used a com- bination strategy, in which hMSCs were seeded on P(VDF-TrFE) or P(VDF-TrFE)/ZnO nanocomposites and allowed to grow for 24 h prior to implantation. The groups of RBCs that were apparent in P(VDF- TrFE)/ZnO scaffolds can be considered the hallmark of enhanced angiogenesis [22]. In the current study, P(VDF-TrFE)/ZnO scaffolds pre-seeded with hMSCs promoted a higher degree of angiogenesis than unseeded scaffolds. The cumulative beneficial effects of piezoelectric

P(VDF-TrFE), ZnO nanoparticles, and hMSCs make the P(VDF-TrFE)/ZnO scaffolds promising candidates for use in tissue engineering.

An illustration of the likely mechanism behind the improved performance of P(VDF-TrFE)/ZnO scaffolds compared to the neat P(VDF-TrFE) scaffolds is shown in Scheme 2. The electric potential generated by piezoelectric P(VDF-TrFE) scaffolds can enhance cell responses [48]. Moreover, ZnO nanoparticles can the scope of this work, it is a critical avenue of future generate reactive ROS like O– and, subsequently, investigation.

The ability of P(VDF-TrFE)/ZnO biomaterials to form well-cellularized scaffolds could improve their function and reduce failure after implantation [60]. Our study demonstrated that P(VDF-TrFE) scaffolds containing less than 4% w/w ZnO nanoparticles were non-toxic to both HUVECs and hMSCs; both cell types had satisfactory viability on neat P(VDF-TrFE), P(VDF-TrFE)/ZnO-1, and P(VDF-TrFE)/ZnO-2 scaffolds, H2O2 [63]. This can enhance cell proliferation [20] and angiogenesis by stimulating the expression of growth factors like VEGF and FGF [22]. Although further studies are required to conclusively determine the causes of improved cell viability, cell adhesion, cell proliferation, and angiogenesis, our results strongly support a major role for both the piezoelectric pro- perties of P(VDF-TrFE) and the redox reactions that occur on the surface of ZnO nanoparticles.

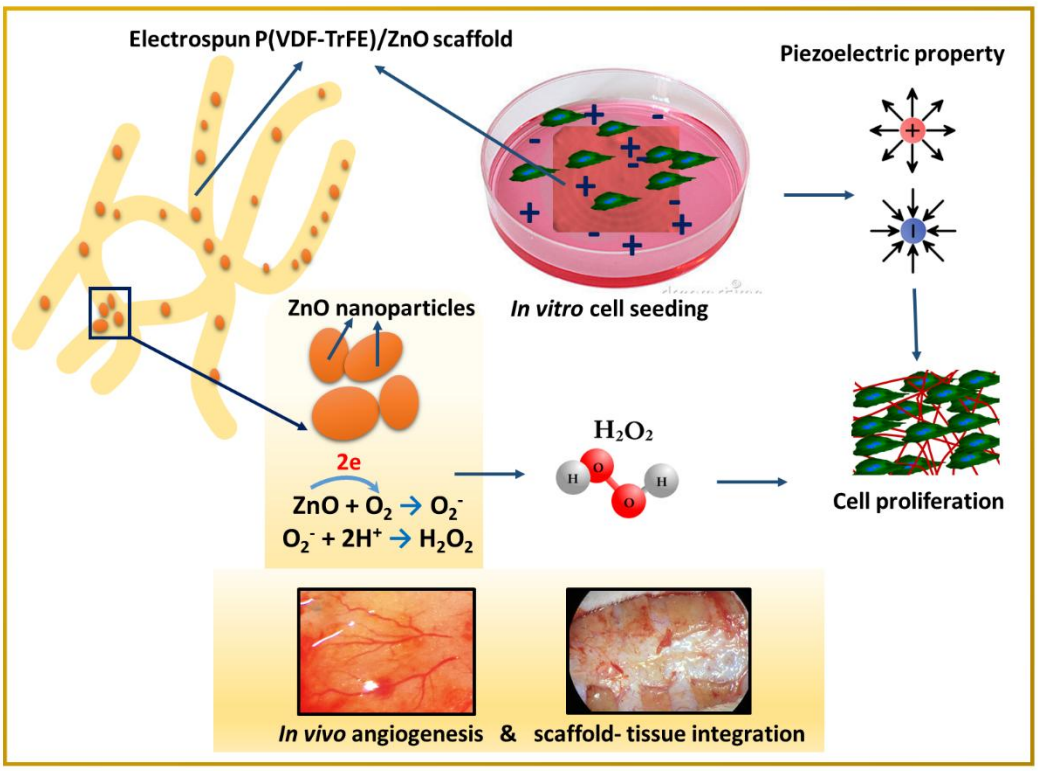

Fig. 8. Schematic illustration of the mechanism of cell proliferation on P(VDF-TrFE)/ZnO nanocomposite scaffolds. Both piezoelectric property of P(VDF-TrFE) and H2O2 molecules released due to ZnO nanoparticles will simultaneously enhance cell proliferation through the scaffolds.

5 Conclusion

Electrospun P(VDF-TrFE)/ZnO nanocomposite scaffolds with various concentrations of ZnO

nanoparticles were fabricated and characterized. SEM, EDS, and XRD analyses confirmed the successful incorporation of ZnO nanoparticles into the P(VDF-TrFE) fiber matrix. It was evident from the SEM micrographs that, at lower filler concentrations, ZnO nanoparticles were well-dispersed in the P(VDF-TrFE) copolymer matrix. However, above 2% w/w, ZnO nanoparticles formed agglomerates in the polymer matrix. Crystalline phase characterization indicated that the P(VDF-TrFE) in the copolymer scaffolds was mainly in the piezoelectric ⊚-phase. All of the scaffolds were highly biocompatible with blood. In vitro cell culture studies using hMSCs and HUVECs showed that the scaffolds were cell- compatible and supported cell adhesion, particularly when the content of ZnO nanoparticles was 2% w/w. Finally, in vivo studies in rats confirmed the non- toxicity of the P(VD-TrFE)/ZnO scaffolds and their ability to promote angiogenesis. Moreover, the presence of ZnO nanoparticles in the scaffolds enhanced angiogenesis and favored more successful integration of the scaffold into the surrounding tissue, which was further boosted by pre-seeding with hMSCs. Collectively, this study suggests that P(VDF-TrFE) containing a low concentration of ZnO nanoparticles could be used as a promising alternative in tissue engineering. However, concerns regarding systemic toxicity, the fate of stem cells on the scaffolds, and long-term patency of the scaffold should be addressed in detail prior to clinical application of the developed material.

Acknowledgements

The authors gratefully acknowledge the financial support of Nancy-Brabois Institute of Technologies, Lorraine University, Nancy, France. The authors also acknowledge the Department of Biotechnology (DBT), Government of India, New Delhi, for the financial support through MSUB IPLSARE Program (No. BT/PR4800/INF/22/152/2012). R. A. thanks the Israel Council for Higher Education for postdoctoral fellowship. P. D. thanks the China scholarship council for overseas fellowship.

References

[1] Kuang, R.; Zhang, Z. P.; Jin, X. B.; Hu, J.; Shi, S. T.; Ni, L. X.; Ma, P. X. Nanofibrous spongy microspheres for the delivery of hypoxia-primed human dental pulp stem cells to regenerate vascularized dental pulp. Acta Biomater. 2016, 33, 225–234.

[2] Briquez, P. S.; Clegg, L. E.; Martino, M. M.; Gabhann, F. M.; Hubbell, J. A. Design principles for therapeutic angiogenic materials. Nat. Rev. Mater. 2016, 1, 15006.

[3] Dondossola, E.; Holzapfel, B. M.; Alexander, S.; Filippini, S.; Hutmacher, D. W.; Friedl, P. Examination of the foreign body response to biomaterials by nonlinear intravital microscopy. Nat. Biomed. Eng. 2016, 1, 0007.

[4] McCaig, C. D.; Song, B.; Rajnicek, A. M. Electrical dimensions in cell science. J. Cell Sci. 2009, 122, 4267–4276.

[5] McCaig, C. D.; Rajnicek, A. M.; Song, B.; Zhao, M. Controlling cell behavior electrically: Current views and future potential. Physiol. Rev. 2005, 85, 943–978.

[6] Weber, N.; Lee, Y. S.; Shanmugasundaram, S.; Jaffe, M.; Arinzeh, T. L. Characterization and in vitro cytocompatibility of piezoelectric electrospun scaffolds. Acta Biomater. 2010, 6, 3550–3556.

[7] Hu, Z. J.; Tian, M. W.; Nysten, B.; Jonas, A. M. Regular arrays of highly ordered

ferroelectric polymer nanostructures for non-volatile low-voltage memories. Nat. Mater. 2009, 8, 62–67.
[8] Huang, S.; Yee, W. A.; Tjiu, W. C.; Liu, Y.; Kotaki, M.; Boey, Y. C. F.; Ma, J.; Liu, T. X.; Lu, X. H. Electrospinning of polyvinylidene difluoride with carbon nanotubes: Synergistic effects of extensional force and interfacial interaction on crystalline structures. Langmuir 2008, 24, 13621–13626.
[9] Li, M. Y.; Wondergem, H. J.; Spijkman, M. J.; Asadi, K.; Katsouras, I.; Blom, P. W. M.; De Leeuw, D. M. Revisiting the δ-phase of poly(vinylidene fluoride) for solution-processed ferroelectric thin films. Nat. Mater. 2013, 12, 433–438.
[10] Liu, Y. W.; Lu, J. F.; Li, H. N.; Wei, J. J.; Li, X. H. Engineering blood vessels through micropatterned co-culture of vascular endothelial and smooth muscle cells on bilayered electrospun fibrous mats with pDNA inoculation. Acta Biomater. 2015, 11, 114–125.
[11] Fine, E. G.; Valentini, R. F.; Bellamkonda, R.; Aebischer, P. Improved nerve regeneration through piezoelectric vinylidenefluoride-trifluoroethylene copolymer guidance channels. Biomaterials 1991, 12, 775–780.
[12] Lee, Y. S.; Collins, G.; Arinzeh, T. L. Neurite extension of primary neurons on electrospun piezoelectric scaffolds. Acta Biomater. 2011, 7, 3877–3886.
[13] Lee, Y. S.; Wu, S.; Arinzeh, T. L.; Bunge, M. B. Enhanced noradrenergic axon regeneration into schwann cell-filled PVDF-TrFE conduits after complete spinal cord transection. Biotechnol. Bioeng. 2017, 114, 444–456.
[14] Martins, P. M.; Ribeiro, S.; Ribeiro, C.; Sencadas, V.; Gomes, A. C.; Gama, F. M.; Lanceros-Méndez, S. Effect of poling state and morphology of piezoelectric poly(vinylidene fluoride) membranes for skeletal muscle tissue engineering. RSC Adv. 2013, 3, 17938–17944.
[15] Hitscherich, P.; Wu, S. L.; Gordan, R.; Xie, L. H.; Arinzeh, T.; Lee, E. J. The effect of PVDF-TrFE scaffolds on stem cell derived cardiovascular cells. Biotechnol. Bioeng. 2016, 113, 1577–1585.
[16] Zhu, P.; Weng, Z. Y.; Li, X.; Liu, X. M.; Wu, S. L.; Yeung, K. W. K.; Wang, X. B.; Cui, Z. D.; Yang, X. J.; Chu, P. K. Biomedical applications of functionalized ZnO nanomaterials: From biosensors to bioimaging. Adv. Mater. Interfaces 2016, 3, 1500494.
[17] Liao, Q. L.; Zhang, Z.; Zhang, X. H.; Mohr, M.; Zhang, Y.; Fecht, H. J. Flexible piezoelectric nanogenerators based on a fiber/ZnO nanowires/paper hybrid structure for energy harvesting. Nano Res. 2014, 7, 917–928.
[18] Kang, Z.; Yan, X. Q.; Zhao, L. Q.; Liao, Q. L.; Zhao, K.; Du, H. W.; Zhang, X. H.; Zhang, X. J.; Zhang, Y. Gold nanoparticle/ZnO nanorod hybrids for enhanced reactive oxygen species generation and photodynamic therapy. Nano Res. 2015, 8, 2004–2014.
[19] Yan, Z. Q.; Zhao, A. D.; Liu, X. P.; Ren, J. S.; Qu, X. G. A pH-switched mesoporous nanoreactor for synergetic therapy. Nano Res. 2017, 10, 1651–1661.
[20] Augustine, R.; Malik, H. N.; Singhal, D. K.; Mukherjee, A.; Malakar, D.; Kalarikkal, N.; Thomas, S. Electrospun polycaprolactone/ZnO nanocomposite membranes as bio-materials with antibacterial and cell adhesion properties. J. Polym. Res. 2014, 21, 347.
[21] Augustine, R.; Dominic, E. A.; Reju, I.; Kaimal, B.; Kalarikkal, N.; Thomas, S. Electrospun polycaprolactone membranes incorporated with ZnO nanoparticles as skin substitutes with enhanced fibroblast proliferation and wound healing. RSC Adv. 2014, 4, 24777–24785.
[22] Augustine, R.; Dominic, E. A.; Reju, I.; Kaimal, B.; Kalarikkal, N.; Thomas, S.

Investigation of angiogenesis and its mechanism using zinc oxide nanoparticle-loaded electrospun tissue engineering scaffolds. RSC Adv. 2014, 4, 51528–51536.
[23] Sirelkhatim, A.; Mahmud, S.; Seeni, A.; Kaus, N. H. M.; Ann, L. C.; Bakhori, S. K. M.; Hasan, H.; Mohamad, D. Review on zinc oxide nanoparticles: Antibacterial activity and toxicity mechanism. Nano-Micro Lett. 2015, 7, 219–242.
[24] Saptarshi, S. R.; Duschl, A.; Lopata, A. L. Biological reactivity of zinc oxide nanoparticles with mammalian test systems: An overview. Nanomedicine 2015, 10, 2075–2092.
[25] Versiani, M. A.; Abi Rached-Junior, F. J.; Kishen, A.; Pécora J. D.; Silva-Sousa, Y. T.; de Sousa-Neto, M. D. Zinc oxide nanoparticles enhance physicochemical characteristics of Grossman sealer. J. Endod. 2016, 42, 1804–1810.
[26] Jiang, L. Y.; Li, Y. B.; Xiong, C. D. Preparation and biological properties of a novel composite scaffold of nano-hydroxyapatite/chitosan/carboxymethyl cellulose for bone tissue engineering. J. Biomed. Sci. 2009, 16, 65.
[27] Joshy, K. S.; Sharma, C. P.; Kalarikkal, N.; Sandeep, K.; Thomas, S.; Pothen, L. A. Evaluation of in-vitro cytotoxicity and cellular uptake efficiency of zidovudine-loaded solid lipid nanoparticles modified with Aloe Vera in glioma cells. Mater. Sci. Eng. C 2016, 66, 40–50.
[28] El Omar, R.; Xiong, Y.; Dostert, G.; Louis, H.; Gentils, M.; Menu, P.; Stoltz, J. F.; Velot, É.; Decot, V. Immunomodulation of endothelial differentiated mesenchymal stromal cells: Impact on T and NK cells. Immunol. Cell Biol. 2015, 94, 342–356.
[29] Choi, Y. Y.; Yun, T. G.; Qaiser, N.; Paik, H.; Roh, H. S.; Hong, J.; Hong, S.; Han, S. M.; No, K. Vertically aligned P(VDF-TrFE) core–shell structures on flexible pillar arrays. Sci. Rep. 2015, 5, 10728.
[30] Tashiro, K.; Takano, K.; Kobayashi, M.; Chatani, Y.; Tadokoro, H. Structural study on ferroelectric phase transition of vinylidene fluoride-trifluoroethylene random copolymers. Polymer 1981, 22, 1312–1314.
[31] Kim, K. J.; Kim, G. B.; Vanlencia, C. L.; Rabolt, J. F. Curie transition, ferroelectric crystal structure, and ferroelectricity of a VDF/TrFE(75/25) copolymer 1. The effect of the consecutive annealing in the ferroelectric state on curie transition and ferroelectric crystal structure. J. Polym. Sci. Part B Polym. Phys. 1994, 32, 2435–2444.
[32] Tashiro, K.; Itoh, Y.; Kobayashi, M.; Tadokoro, H. Polarized Raman spectra and LO-TO splitting of poly (vinylidene fluoride) crystal form I. Macromolecules 1985, 18, 2600–2606.
[33] Mattsson, B.; Ericson, H.; Torell, L. M.; Sundholm, F. Micro-Raman investigations of PVDF-based proton-conducting membranes. J. Polym. Sci. Part A Polym. Chem. 1999, 37, 3317–3327.
[34] Yee, W. A.; Nguyen, A. C.; Lee, P. S.; Kotaki, M.; Liu, Y.; Tan, B. T.; Mhaisalkar, S.; Lu, X. H. Stress-induced structural changes in electrospun polyvinylidene difluoride nanofibers collected using a modified rotating disk. Polymer 2008, 49, 4196–4203.
[35] Mahdi, R. I.; Gan, W. C.; Abd Majid, W. H. Hot plate annealing at a low temperature of a thin ferroelectric P(VDF-TrFE) film with an improved crystalline structure for sensors and actuators. Sensors 2014, 14, 19115–19127.
[36] Xu, B.; Choi, J.; Borca, C. N.; Dowben, P. A.; Sorokin, A. V.; Palto, S. P.; Petukhova, N. N.; Yudin, S. G. Comparison of aluminum and sodium doped poly(vinylidene fluoride-trifluoroethylene) copolymers by X-ray photoemission spectroscopy. Appl. Phys. Lett. 2001, 78, 448–450.
[37] Nguyen, V. S.; Rouxel, D.; Vincent, B.; Badie, L.; Dos Santos, F. D.; Lamouroux, E.;

Fort, Y. Influence of cluster size and surface functionalization of ZnO nanoparticles on the morphology, thermomechanical and piezoelectric properties of P(VDF-TrFE) nanocomposite films. Appl. Surf. Sci. 2013, 279, 204–211.
[38] Bharti, V.; Xu, H. S.; Shanthi, G.; Zhang, Q. M.; Liang, K.
M. Polarization and structural properties of high-energy electron irradiated poly(vinylidene fluoride-trifluoroethylene) copolymer films. J. Appl. Phys. 2000, 87, 452–461.
[39] Oswald, J.; Boxberger, S.; Jørgensen, B.; Feldmann, S.; Ehninger, G.; Bornhäuser M.; Werner, C. Mesenchymal stem cells can be differentiated into endothelial cells in vitro. Stem Cells 2004, 22, 377–384.
[40] Lutolf, M. P.; Hubbell, J. A. Synthetic biomaterials as instructive extracellular microenvironments for morphogenesis in tissue engineering. Nat. Biotechnol. 2005, 23, 47–55.
[41] Place, E. S.; Evans, N. D.; Stevens, M. M. Complexity in biomaterials for tissue engineering. Nat. Mater. 2009, 8, 457–470.
[42] Okoshi, T.; Chen, H.; Soldani, G.; Galletti, P. M.; Goddard,
M. Microporous small diameter PVDF-TrFE vascular grafts fabricated by a spray phase inversion technique. ASAIO J. 1992, 38, M201–M206.
[43] Katsouras, I.; Asadi, K.; Li, M. Y.; Van Driel, T. B.; Kjær,
K. S.; Zhao, D.; Lenz, T.; Gu, Y.; Blom, P. W. M.; Damjanovic, D. et al. The negative piezoelectric effect of the ferroelectric polymer poly(vinylidene fluoride). Nat. Mater. 2016, 15, 78–84.
[44] Zhang, X. H.; Zhang, C. G.; Lin, Y. H.; Hu, P. H.; Shen, Y.; Wang, K.; Meng, S.; Chai, Y.; Dai, X. H.; Liu, X. et al. Nanocomposite membranes enhance bone regeneration through restoring physiological electric microenvironment. ACS Nano 2016, 10, 7279–7286.
[45] Zhang, D.; Karki, A. B.; Rutman, D.; Young, D. P.; Wang, A.; Cocke, D.; Ho, T. H.; Guo, Z. H. Electrospun polyacrylonitrile nanocomposite fibers reinforced with Fe3O4 nanoparticles: Fabrication and property analysis. Polymer 2009, 50, 4189– 4198.
[46] Baumgarten, P. K. Electrostatic spinning of acrylic microfibers. J. Colloid Interface Sci. 1971, 36, 71–79.
[47] Huttenlocher, A.; Horwitz, A. R. Wound healing with electric potential. N. Engl. J. Med. 2007, 356, 303–304.
[48] Hwang, G. T.; Byun, M.; Jeong, C. K.; Lee, K. J. Flexible piezoelectric thin-film energy harvesters and nanosensors for biomedical applications. Adv. Healthc. Mater. 2015, 4, 646–658.
[49] Lonjon, A.; Laffont, L.; Demont, P.; Dantras, E.; Lacabanne,
C. Structural and electrical properties of gold nanowires/ P(VDF-TrFE) nanocomposites. J. Phys. D: Appl. Phys. 2010, 43, 345401.
[50] Andrew, J. S.; Clarke, D. R. Effect of electrospinning on the ferroelectric phase content of polyvinylidene difluoride fibers. Langmuir 2008, 24, 670–672.
[51] Guo, H. F.; Li, Z. S.; Dong, S. W.; Chen, W. J.; Deng, L.; Wang, Y. F.; Ying, D. J. Piezoelectric PU/PVDF electrospun scaffolds for wound healing applications. Colloids Surf. B: Biointerfaces 2012, 96, 29–36.
[52] Augustine, R.; Sarry, F.; Kalarikkal, N.; Thomas, S.; Badie, L.; Rouxel, D. Surface acoustic wave device with reduced insertion loss by electrospinning P(VDF-TrFE)/ZnO nano- composites. Nano-Micro Lett. 2016, 8, 282–290.
[53] Lee, Y. S.; Arinzeh, T. L. The influence of piezoelectric scaffolds on neural differentiation of human neural stem/ progenitor cells. Tissue Eng. Part A 2012, 18, 2063–

2072.
[54] Li, W. J.; Laurencin, C. T.; Caterson, E. J.; Tuan, R. S.; Ko, F. K. Electrospun nanofibrous structure: A novel scaffold for tissue engineering. J. Biomed. Mater. Res. 2002, 60, 613–621.
[55] Chhabra, H.; Deshpande, R.; Kanitkar, M.; Jaiswal, A.; Kale, V. P.; Bellare, J. R. A nano zinc oxide doped electrospun scaffold improves wound healing in a rodent model. RSC Adv. 2016, 6, 1428–1439.
[56] Augustine, R.; Mathew, A.; Sosnik, A. Metal oxide nano- particles as versatile therapeutic agents modulating cell signaling pathways: Linking nanotechnology with molecular medicine. Appl. Mater. Today 2017, in press.
[57] Paszek, E.; Czyz, J.; Woźnicka, O.; Jakubiak, D.; Wojnarowicz, J.; Łojkowski, W.; Stępień, E. Zinc oxide nanoparticles impair the integrity of human umbilical vein endothelial cell monolayer in vitro. J. Biomed. Nanotechnol. 2012, 8, 957–967.
[58] Hsiao, I. L.; Huang, Y. J. Effects of various physicochemical characteristics on the toxicities of ZnO and TiO2 nanoparticles toward human lung epithelial cells. Sci. Total Environ. 2011, 409, 1219–1228.
[59] Nair, S.; Sasidharan, A.; Divya Rani, V. V.; Menon, D.; Nair, S.; Manzoor, K.; Raina, S. Role of size scale of ZnO nanoparticles and microparticles on toxicity toward bacteria and osteoblast cancer cells. J. Mater. Sci.: Mater. Med. 2009, 20, 235.
[60] Mironov, V.; Kasyanov, V.; Markwald, R. R. Nanotechnology in vascular tissue engineering: From nanoscaffolding towards rapid vessel biofabrication. Trends Biotechnol. 2008, 26, 338–244.
[61] Barui, A. K.; Veeriah, V.; Mukherjee, S.; Manna, J.; Patel, A. K.; Patra, S.; Pal, K.; Murali, S.; Rana, R. K.; Chatterjee, S. et al. Zinc oxide nanoflowers make new blood vessels. Nanoscale 2012, 4, 7861–7869.
[62] Todeschi, M. R.; El Backly, R.; Capelli, C.; Daga, A.; Patrone, E.; Introna, M.; Cancedda, R.; Mastrogiacomo, M. Transplanted umbilical cord mesenchymal stem cells modify the in vivo microenvironment enhancing angiogenesis and leading to bone regeneration. Stem Cells Dev. 2015, 24, 1570–1581.
[63] Hoffman, A. J.; Carraway, E. R.; Hoffmann, M. R. Photocatalytic production of H2O2 and organic peroxides on quantum-sized semiconductor colloids. Environ. Sci. Technol. 1994, 28, 776–785.